Toughness of 12%Cr Ferritic/Martensitic Steel Welds Produced by Non-Arc Welding Processes

Martensitic structure gives best fusion weld toughness for low-cost stainless steels, while friction welding can be advantageous for more ferritic alloys

BY B. J. GINN AND T. G. GOOCH

ABSTRACT. Low carbon 12%Cr steels can offer reduced life cycle costs in many applications. The present work examined the behavior of commercial steels of varying composition when subject to low heat input welding by the electron beam (EB) process and to a forge cycle by linear friction welding (LFW). Charpy impact testing was carried out on the high temperature heat-affected zone (HAZ)/fusion boundary or weld interface, with metallographic examination.

With EB welding, the ductile-brittle transition temperature (DBTT) was below 0°C (32°F) only for steel of low ferrite factor giving a fully martensitic weld area. Higher ferrite factor alloys showed predominantly ferritic transformed microstructures and a transition well above room temperature. Grain coarsening was found even with low EB process power, the peak grain size increasing with both heat input and steel ferrite factor. Use of LFW gave a fine weld area structure and DBTTs around 0°C even in high ferrite factor (FF) material.

Introduction

Components manufactured from austenitic stainless steel are initially more expensive than comparable items manufactured from carbon steel. However, in some cases, the increased production costs can be recouped by improved corrosion resistance, and hence, longer service life. In recent years, interest has developed in low carbon 11–12%Cr dual phase ferritic/martensitic steels (Ref. 1). Although not strictly "stainless steels" because they develop a rust coating in a humid atmosphere, the rate at which their degradation occurs is considerably slower than for carbon steels. Production costs are lower than for austenitic grades because such steels have reduced Ni contents (<0.5%) and can be manufactured using rolling mills and equipment appropriate to plain ferritic steels.

Conventional 12%Cr alloys have a martensitic structure and weldments will normally require both preheat, if hydrogen cracking is to be prevented, and postweld heat treatment to improve toughness (Ref. 2). Lowering the carbon content to below approximately 0.1% avoids these measures. However, this promotes a ferritic structure (Ref. 3), which leads to severe grain growth in the temperature range associated with welding, and hence, local loss of toughness. Manufacturers of 12%Cr steels have therefore attempted to balance the extremes of behavior associated with completely martensitic or ferritic materials by careful compositional control to produce duplex ferrite/martensite alloys. However, the first generation of such 12%Cr steels still suffered HAZ grain coarsening on welding, which resulted in reduced toughness (Ref. 4). While refinements to the chemical composition by various manufacturers have reduced this tendency in current steels, concern remains over reduced HAZ toughness and increased HAZ hardness levels. Previous work on shielded metal arc (SMA) welds concluded that, for steels in which ferrite was the major HAZ phase, increasing martensite had a slightly detrimental effect on toughness (Ref. 4), but that HAZ toughness was dependent mainly upon the peak ferrite grain size produced by welding. More recently, it has become clear that alloys with composition balanced to provide a fully martensitic structure render better HAZ toughness, although with inevitable hardening in the weld area (Ref. 5).

The low carbon 12%Cr steels are available in a variety of product forms, *i.e.*, plate, sheet and coil, in thicknesses from 1 mm to in excess of 30 mm. However, it is likely that future applications will concentrate on material thicknesses below 10 mm. Whereas the arc welding characteristics of 12%Cr ferritic/martensitic alloys have been examined (Refs. 4–6), there appear to be no data on high-speed power beam processes or on forge welding, which may reduce the tendency to form coarse-grained HAZs, and can further offer advantage in higher joint completion rates for a variety of engineering fabrications. The present study, therefore, applied electron beam (EB) and linear friction welding (LFW) to a range of commercial steels. The weld zone properties were determined by metallurgical examination, hardness measurement and impact toughness testing.

KEY WORDS

Electron Beam Welding
Linear Friction Welding
Ferritic/Martensitic
Stainless Steel
Charpy Impact Testing
Heat-Affected Zone
Impact Toughness

Experimental Program

Materials

Five different heats of 12%Cr ferritic/martensitic stainless steel were assessed. Three of these (identified here as 1C849, 1C850 and 1C857, and supplied by different manufacturers), were nominally 6 mm thick and were representative

B. J. GINN and T. G. GOOCH are with TWI, Abington Hall, Abington, Cambridge, U.K.

of material currently available. The remaining two materials (1C492 and 1C495) were examples of earlier grades and were 12 mm thick. The chemical compositions of all five materials were determined by optical emission spectrometry (OES) for the major elements and by combustion in oxygen and inert gas fusion techniques for C, O and N. The chemical compositions are reported in Table 1; the mechanical properties given in the manufacturers' data sheets are reported in Table 2.

The influence of variations in alloying additions on the steel microstructure can be assessed by calculation of the Kaltenhauser Ferrite Factor (FF) (Ref. 7):

$$FF = \%Cr + 6\%Si + 8\%Ti + 4\%Mo + 2\%Al + 4\%Nb - 2\%Mn - 4\%Ni - 40\,(\%C + N).$$

A higher FF value indicates greater ferrite stability. In terms of microstructures formed during welding, on cooling from the melting point, less austenite forms. Therefore, the final martensite content is reduced. The FF values for the five steels are given in Table 1 and cover the range 7.8–11.2.

Welding Procedure

Melt runs were produced using the EB process with a range of welding parameters and resultant cooling rates (Table 3). The melt runs in the 6-mm-thick material were made using an assembly consisting of two matching plates clamped together, with the lower plate acting as a backing bar. The use of a backing bar was not necessary when melt runs were made on the two thicker materials.

Linear friction welds using rectangular samples 200 mm wide were produced from the 6-mm-thick materials. The machine parameters employed are reported in Table 4.

Butt joints were made by the shielded metal arc (SMA) process in one low ferrite factor (1C849) material for comparison with earlier work (Ref. 4). The K-type weld preparation had an included angle of 60 deg and used a type 309 austenitic filler. Welding conditions are given in Table 5.

Metallography

Transverse sections were taken from all weldments produced. In addition, selected EB welds and Charpy samples were sectioned in a plane parallel to the plate surface. The sections were prepared for examination by polishing on diamond laps and etching in Vilella's reagent (2 g picric acid, 10 mls hydrochloric acid and 200 mls methyl alcohol). The ferrite grain size was determined in the high-temperature grain-coarsened HAZ evident on the transverse sections for the various E8 conditions. The percentage of martensite present was calculated from measurements made using a linear intercept technique.

Mechanical Testing

Vickers hardness measurements were made, employing a 2.5-kg load, on the base materials and high-temperature HAZs/fusion zones produced by the electron beam runs. For the linear friction joints, measurements were taken on the weld interface and in the HAZ.

Transverse sub size (5 mm thick) Charpy impact specimens were machined from the welded samples. The specimens were notched nominally on the fusion boundary or weld interface, through the plate thickness, so that crack growth was parallel to the welding direction. Testing was carried out over a range of temperatures from −80 to 200°C (−112 to 392°F), to define the ductile/brittle transition, with seven to ten samples being tested per weld.

Results

Chemical Composition

From Table 1, only slight differences are noted among the five steels with regard to most elements. The two earlier

Table 1 — Chemical Compositions of Base Steels with Manufacturers' Specifications

Material Identity	C	S	P	Si	Mn	Ni	Cr	Ti	N	FF
	Element wt.%									
1C849	0.016 0.03 max	0.004 0.02 max	0.015 0.04 max	0.40 0.50 max	1.15 0.5–2.5	0.50 0.3–1.0	11.0 10.5–12.5	0.01 —	0.018 0.03 max	7.8 —
1C850	0.015 0.03 max	0.005 0.03 max	0.021 0.04 max	0.48 1.0 max	0.98 1.5 max	0.12 1.5 max	11.5 10.5–12.0	<0.01 0.6 max	0.016 0.03 max	11.1 11 max
1C857	0.009 0.03 max	0.003 —	0.019 —	0.50 1.0 max	1.14 2.0 max	0.69 1.5 max	11.8 11.0–12.0	0.27 4x(C+N) 0.6 max	0.013 —	11.2 —
1C492	0.022 0.03 max	0.019 0.03 max	0.022 0.03 max	0.45 1.0 max	1.32 1.5 max	0.61 1.5 max	11.4 11.0–12.0	0.29 0.6 max	0.017 —	9.7 —
1C495	0.025 0.03 max	0.009 0.03 max	0.019 0.03 max	0.34 1.0 max	1.23 1.5 max	0.56 1.5 max	11.4 11.0–12.0	0.42 0.6 max	0.010 —	10.8 —

— = not specified

Table 2 — Mechanical Properties of Base Metals

Material Identity	0.2 Proof Stress, N/mm2(a)	Tensile Strength, N/mm2(a)	Elongation, % min.(a)	Hardness, (Vickers)(a)	Impact Energy, J at 20°C (68°F)(b)
1C849	320 min.	450–600	20	160 approx	64–68
1C850	280 min.	460 min.	20	232 max	43–46
1C857	280 min.	460 min.	20	230 max	54–55
1C492	280 min.	460 min.	20	190 max	50–50
1C495	280 mm	460 min.	20	190 max	44–46

(a) Manufacturers' data.
(b) Measured on 10 x 5 mm Charpy samples.

Table 3 — Electron Beam Welding Conditions

Voltage, kV	Current, mA	Welding Speed, mm/min	Process Power, kJ/mm
130	40	2250	0.1
130	30	1000	0.2
130	20	500	0.3
130	16	200	0.6
130	16	115	1.1

Table 4 — Linear Friction Welding Conditions

Oscillation amplitude and frequency:	600 Hz, 2.2 mm
Burn-off force:	11 kN
Burn-off time:	1.85 s
Burn-off:	4 mm
Forge force:	13 kN
Hold time:	10 s

Table 5— SMA Butt Joint Weld Conditions: 2.5-mm-Diameter Electrodes

Location	Voltage, V	Current, A	Travel Speed, mm/min	Arc Energy, kJ/mm
Root	27	59	140	0.7
Fill	26	70	160	0.7

generation steels, 1C492 and 1C495, had slightly higher carbon contents than the current grades. The ranges of Cr content cited hy the various manufacturers varied somewhat, but the measured contents ranged only from 11.0 to 11.8%. Steel 1C850 had the lowest Ni level at 0.12%, with the other four grades ranging from 0.5% in steel 1C849 to 0.69% in steel 1C857. Steels 1C849 and 1C850 did not contain any measurable Ti, while the other three varied from 0.27% in 1C857 to 0.42% in steel 1C495.

The range in FF values in Table 1 reflects the variation in alloying additions. It is not possible to separate old and new grades based solely on this empirical relationship, although the recent grade 1C849 was noted to have the lowest FF value (*i.e.*, 7.8).

Metallurgical Examination

Base Steel

Figure 1 shows base metal microstructures. In each case, these appeared to be fully ferritic, regions of tempered martensite not being clearly distinguishable, but there were considerable variations in grain size. Steels 1C849 and 1C850 showed the finest grain size (about 20 μm diameter), while steel 1C857 was the coarsest (60 μm) and contained regular-shaped particles, presumed to be Ti(C, N). Materials 1C492 and 1C495 had grain sizes between these two extremes, about 40 μm, and again contained particles of Ti(C, N).

Electron Beam Welds

The microstructures evident on transverse sections varied depending upon the steel type (Fig. 2) and process power employed (Fig. 3), in terms of weld area ferrite grain size (Table 6) and martensite content (Table 7). In steel 1C849, the HAZ and weld metal were fully martensitic (Fig. 2A) for all process power conditions examined, with a prior austenite grain size above that of base metal. The other alloys showed predominantly ferritic weld areas. The weld metal had solidified epitaxially from the high-temperature HAZ; in consequence, the exact location of the fusion boundary was difficult to define, being manifest only as a transition between equiaxed and more columnar grain morphology. Steel 1C850 showed only 6.5% martensite in the HAZ at low power, although the content progressively increased with higher energies, reaching about 35% at 1.1 kJ/mm. The martensite content of steel 1C857 also increased with process power (Fig. 3), but up to only 5%.

Figure 4 was derived from Table 6,and illustrates that the peak HAZ ferrite grain size increased over the power range explored. For the finest grained material (*i.e.*, 1C850, FF 10.8), even at low power the peak ferrite grain diameter was doubled, compared to the base microstructure. However, the degree of ferrite grain coarsening was least for the low FF alloy 1C492.

Accurate measurement of the average ferrite grain size in the EB melt zones proved problematic due to the columnar structure. Nevertheless, similar trends as in the HAZs were noted both in the martensite-forming tendency of the different material types at specific power conditions (Fig. 5) and in that the ferrite grain size increased with process power, approximately doubling over the range examined. In most cases, the columnar weld metal grains had formed roughly perpendicular to the fusion boundary, giving a clear weld centerline. However, in the higher power weldments, some areas displayed nucleation of grains from the back edge of the pool at the weld center, with growth parallel to the welding direction — Fig. 6. On a plan section, the resultant grains were greatly elongated and up to roughly 2 mm in length.

Linear Friction Welds

Examination of microsections at the midpoint of the linear friction welds indicated that the weld zone could be divided into two distinct regions, a narrow weld interface and a HAZ, which increased in visible width toward the material surface — Fig. 7. The structure in the weld region was extremely fine, and it was not possible to resolve ferrite and martensite optically — Fig. 8.

SMA Weld

The HAZ microstructure of the SMA weld in the low ferrite factor steel 1C849 was fully martensitic. In the reheated center plate region — the area from which the reduced section impact specimens were machined — the apparent austenite grain size was considerably finer than that of the capping passes at the surface of the plate, where larger grains were evident, comparable to the EB weld in Fig. 2A. In the former area, the grain size in fact appeared similar in size to that produced by linear friction welding.

Hardness Testing

The base metals showed broadly similar hardneses, steel 1C495 having the highest average hardness of 169 HV and 1C857 the lowest at 156 HV. For the EB samples, HAZ and melt-zone hardness was generally above base steel level (Table 8) and tended to fall slightly with increasing process power, more especially for the higher FF steels. Highest

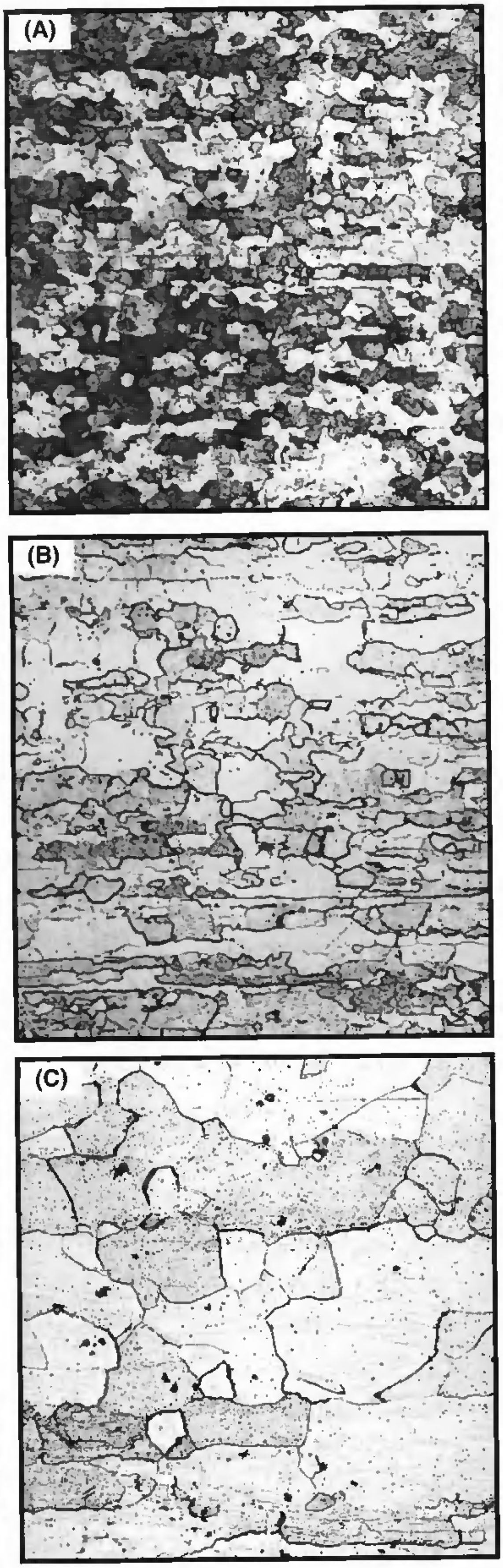

Fig. 1 — Base metal microstructures (400X). A — 1C849 (FF 7.8); B — 1C850 (FF 10.8); and C — 1C857 (FF 11.2).

Fig. 2 — Effect of FF on EB HAZ microstructure (400X). A — 1C849 (FF 7.8); B — 1C850 (FF 10.8).

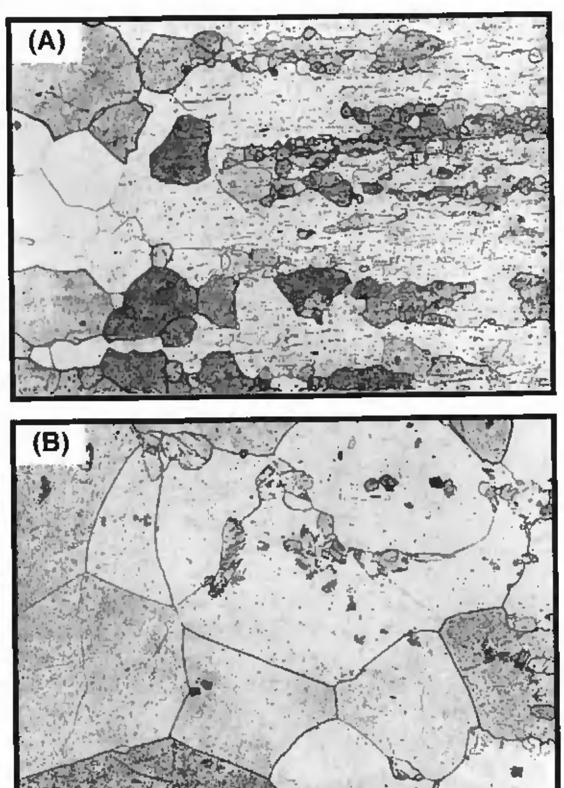

Fig. 3 — Effect of process power on EB HAZ grain growth and martensite formation: 1C857 (FF 11.2) (400X). A — 0.1 kJ/mm; B — 1.1 kJ/mm.

hardness was evident for the low FF steel, 1C849. In the linear friction welds, considerable hardening occurred along the weld interface, particularly for steel 1C849.

Impact Tests

The Charpy tests on individual welds showed the expected transition from low to high absorbed energy as the test temperature was increased. In the samples examined, crack growth from the notch generally took place close to the fusion boundary in the high-temperature HAZ and adjacent weld metal, although the exact location of the crack path could not be defined in view of the continuity of grain structure across the fusion boundary. Some scatter in the transition region was observed, most especially for the EB welds. The individual Charpy samples were examined for the different steels, with particular attention to "outliers." Two particular trends were noted. First, some samples showing relatively high absorbed energy at temperatures below the "average" transition displayed lateral deviation of the crack away from the notch, with growth in the low-tempeature HAZ and adjacent base metal. Second, outlying points corresponding to low absorbed energy at fairly high tempera-

Table 6 — EB HAZ Ferrite Grain Size Measured on Transverse Sections

Material Identity	Base Metal	Grain Size, μm[a] Process Power, kJ/mm 0.1	0.2	0.3	0.6	1.1
1C492	25 – 65[b] / 43	22 – 65 / 38	22 – 65 / 40	30 – 90 / 55	30 – 90 / 57	30 – 70 / 55
1C495	30 – 45 / 37	13 – 45 / 25	19 – 110 / 47	30 – 90 / 58	19 – 110 / 56	45 – 180 / 107
1C849	16 – 22 / 19	(c)	(c)	(c)	(c)	(c)
1C850	16 – 30 / 23	22 – 65 / 46	45 – 90 / 70	45 – 65 / 55	30 – 130 / 69	45 – 130 / 80
1C857	30 – 90 / 60	22 – 90 / 52	22 – 90 / 59	30 – 130 / 43	30 – 130 / 43	65 – 250 / 104

(a) Expressed as diameter of average cross section
(b) Results taken over six readings and presented in the form: Range / Mean
(c) Not determined, as fully martensitic structure

Table 7 — EB Weldment Martensite Contents

Material Identity	Martensite Content (%) Process Power, kJ/mm 0.1	0.2	0.3	0.6	1.1
1C492	8.5	13	6.5	26	28
1C495	0	1.5	1.0	3.5	9.5
1C849	100	100	100	100	100
1C850	6.5	17	42	37	36
1C857	0	1.0	3.0	1.0	5.0

200 counts per sample

ture were noted principally for the medium- to high-process power welds. Examination of sections taken parallel to the plate surface showed that these samples corresponded to crack propagation along the weld centerline in grains elongated in the welding direction — Fig. 9.

Results for the EB process are illustrated by Fig. 10 for a process power of 0.1 kJ/mm. Notwithstanding the scatter, the only material giving a transition below 0°C was the fully martensitic steel 1C849. Increasing EB process power gave a general increase in the transition temperature, as shown in Fig. 11. For material 1C849, 0.1 kJ/mm gave a transition at around –30°C (–22°F), and at about 10°C (50°F) for 0.6 kJ/mm (Fig. 11A), although the higher power resulted in greater upper shelf energy absorption. Figure 11B compares transition curves for steel 1C850; again, lower heat input reduced the transition temperature range. From the EB Charpy tests, approximate ductile-brittle transition temperatures (DBTT) were obtained for an absorbed energy of 15 J, this value corresponding to a level of 30 J for a full-sized sample (Ref. 4). These data are given in Table 9. The highest DBTT was apparently found for steel 1C492, but the fracture faces showed porosity on one side, probably because sample machining inadvertently included the weld root region.

The impact test results from the linear friction welds are presented in Fig. 12. The three grades tested follow a similar order as for the EB runs, 1C849 offering the best toughness. The other steels showed higher and comparable DBTTs, but these were lower than obtained in EB samples.

Figure 13 gives the impact values obtained for the HAZ regions of the SMA butt joint weld in steel 1C849. These indicate a DBTT at around –70°C (–94°F) and absorbed energy values above 0°C of about 100 J, the DBTT being appreciably below that obtained previously for the higher FF steel 1C495 (Ref. 4), although it will be noted that the latter tests employed full-sized Charpy samples.

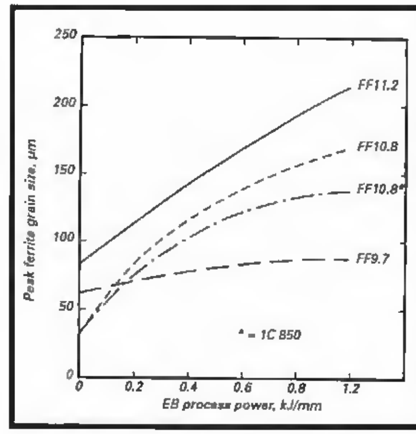

Fig. 4 — Effect of process power on EB weld peak HAZ grain size.

Discussion

Weld Area Microstructure

The EB welds clearly showed the effect of steel FF in determining the transformed structure in the weld area. The low ferrite factor material gave a fully martensitic weld region for the welding conditions employed, whereas the other steels displayed retention of the high temperature ferrite phase and only limited formation of intergranular martensite. With the higher FF steels, the martensite content increased with process power, indicating a greater degree of transformation to austenite during the associated slower cooling from above the A_4 temperature. From Table 7, the empirical FF relationship derived for base metal does not describe the tendency to form martensite on welding entirely consistently. The situation is illustrated by Fig. 14, which is a compilation of the present and other data obtained at TWI. Nevertheless, the FF term is a useful descriptor of HAZ structure, and, in particular, the sharp transition in weld area microstructure at about FF = 9 is evident, corresponding to the nose of the gamma loop in the Fe-Cr system (Ref. 8).

Noting that the base metals varied considerably in initial grain size, the extent of grain growth was influenced by the ferrite factor, presumably via its effect on the A_4 temperature and the size of the austenite range; grain growth was most pronounced in steels of highest ferrite factor that would have the widest ferrite range and lowest A_4 temperature. Earlier work (Ref. 4) examined the rate of ferrite grain growth above the A_4 point. The present steels constitute a wider range of FF, and, using the same relationship (Ref. 4), lowering the A_4 from 130°C to 1150°C (2462°F to 2102°F) (*i.e.*, FF from 9.7 to

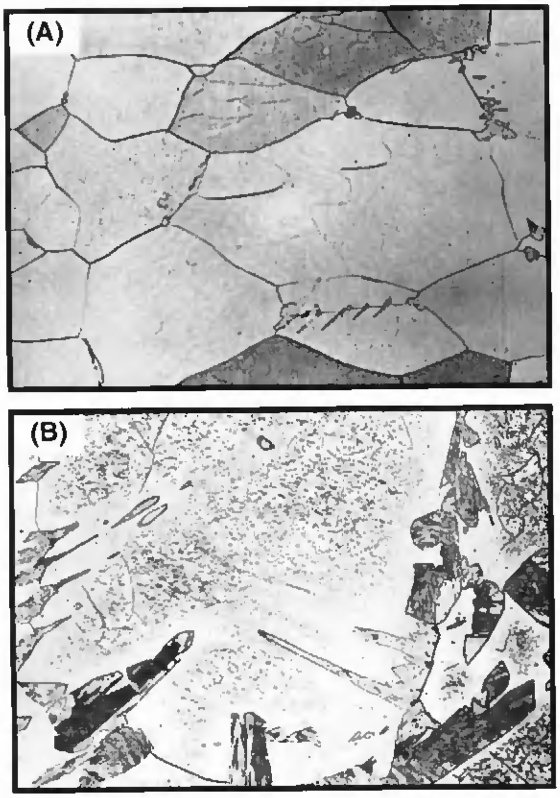

Fig. 5 — E8 fused zone microstructures on transverse sections: 1C850 (FF 10.8) (400X). A — 0.1 kJ/mm; B — 1.1 kJ/mm.

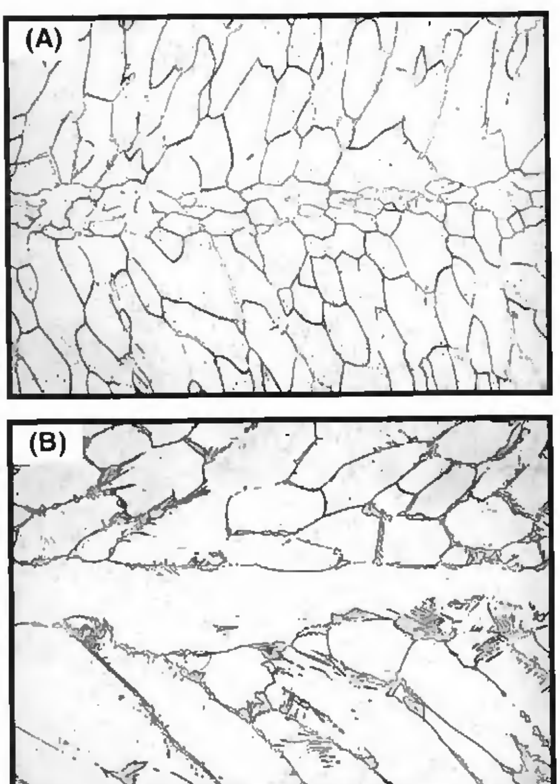

Fig. 6 — Centerline structures in E8 welds: 1C850 (FF 10.8) (50X). A — 0.3 kJ/mm; B — 0.6 kJ/mm.

11.2) would increase the amount of grain growth by roughly a factor of 5, commensurate with the trend in Fig. 4.

In principle, the low heat input available from power beam welding processes is of benefit in minimizing HAZ grain coarsening, although epitaxial solidification of weld metal means that grain size in the fused zone can be fairly large. A previous study on arc welds (Ref. 4) showed that very low heat input is necessary to avoid HAZ grain growth in high FF steels of the present type. The present data support this view in that appreciable grain growth was evident even at only 0.2 kJ/mm electron beam power.

The development of stable grain growth parallel to the welding direction from the back edge of a weld pool has been variously observed (Ref. 9). It has been associated especially with the electron beam process, and the controlling factor has been found to be travel speed, the effect being suppressed by high-speed welding (Ref. 9). The present study is consistent with other work in that such a solidification structure was not observed in the low process power samples, which were produced at the highest travel speed. This is likely to be a geometric effect, dependent on pool shape. Recognizing that the profile of the fused zone will vary through the steel thickness (Ref. 10), the teardrop shape resulting from high travel speed will prevent nucleation of solidifying grains from the back edge of the pool so that an elongated centerline structure will be suppressed. The transition may reflect a kinetic limitation on solidification velocity parallel to the welding direction, but this is unlikely. Direct measurement on electron beam and arc welds indicates solidification velocities up to some 300 mm/min, *i.e.*, similar to the travel speeds found to prevent centerline growth (Ref. 10). However, the maximum solidification velocity depends on pool superheat and

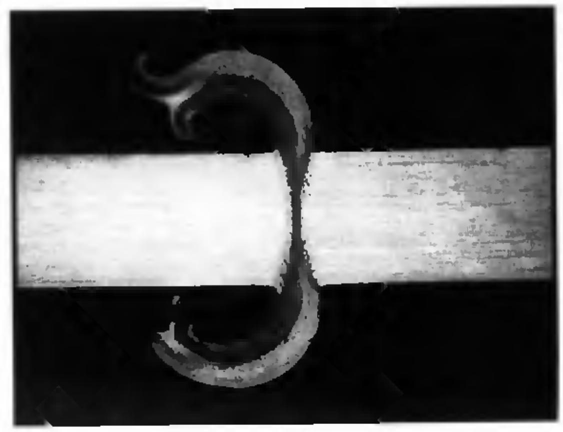

Fig. 7 — Section through linear friction weld: 1C857 (FF 11.2) (5X).

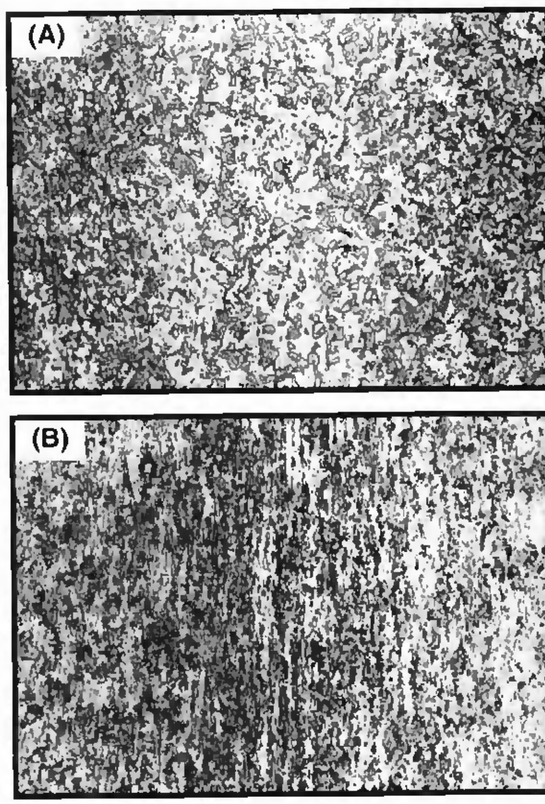

Fig. 8 — Weld interface LFW structures (400X). A — 1C849 (FF 7.8); B — 1C857 (FF 11.2).

Table 8 — Summary of Vickers Hardness Results

Material	FF	Maximum Hardness, HV5 BM	EB* HAZ	EB* WM	LFW
1C492	9.7	174	212	190	—
1C495	10.8	181	183	177	—
1C849	7.8	186	327	320	327
1C850	10.8	177	224	229	314
1C857	11.2	159	179	174	270

*0.3 kJ/mm

Table 9 — Ductile-Brittle Transition Temperatures for EB Welds

Steel	15-J Transition Temperature, °C 0.1 kJ/mm	0.2 kJ/mm	0.3 kJ/mm	0.6 kJ/mm	1.1 kJ/mm
1C492	(110)	—	—	—	—
1C495	45	—	—	—	—
1C849	−40	—	—	10	—
1C850	40	45	35	65	75
1C857	45	—	—	65	—

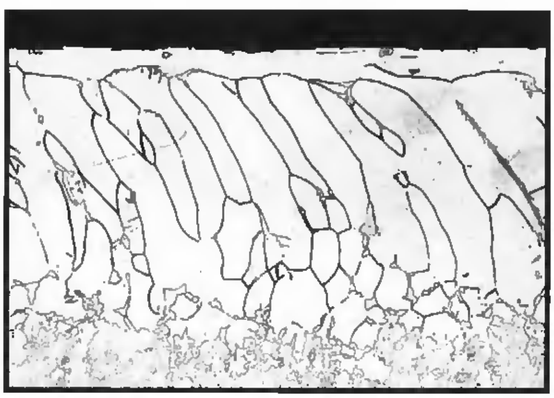

Fig. 9 — Crack propagation in EB Charpy sample along centerline grain. Fracture face at top of illustration: 1C850 (FF 10.8), 0.3 kJ/mm (100X).

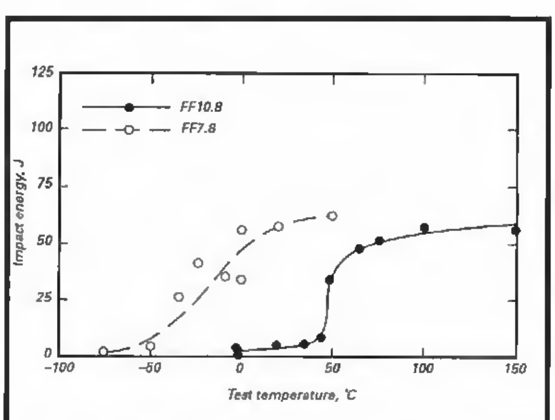

Fig. 10 — Charpy impact results for EB welds in 1C849 (FF 7.8) and 1C495 (FF 10.8): 0.1 kJ/mm.

heat flux across the fusion boundary and is thus a function of the beam power density. At 0.3 kJ/mm, the present power density was about 10^{9} W/m^2. Following the analysis of Hsu, *et al.* (Ref. 11), this would correspond to a maximum achievable solidification velocity of some 5000 mm/min, well above the travel speed of 500 mm/min.

Turning to the linear friction welds, the major feature is that the process resulted in a very fine structure in the bond area. This was found in all cases, regardless of ferrite factor. The degree of cold working indicated by the local hardening precluded detailed examination of the structure, but clearly ferrite grain coarsening can be effectively obviated by the forge stage during welding.

Weld Area Toughness

Other work has shown the potential improvement in toughness at fusion welds afforded by use of alloys with low ferrite factor and transformation to martensite in the weld area (Refs. 5, 6). The present EB and SMA results confirm this trend and illustrate the advantage of obtaining a low carbon martensite structure on welding. For the higher ferrite factor steels, all transformation temperatures obtained, even on the 5-mm-thick samples tested, were significantly above normal ambient. On the other hand, the LFW data demonstrate the benefit of a forge stage to give structural refinement during welding, and even with high ferrite factor material it is possible to achieve a joint transition temperature of around 0°C or below. This was obtained despite the localized work hardening and reorientation of second-phase particles during forging.

Accepting that a transverse section does not fully describe three-dimensional grain morphology, Fig. 15 shows that, for welds where a transition temperature for the fusion boundary region could be determined, the DBTT displayed a similar influence of measured grain size to that found for arc welds: Coarse grain size is detrimental. The possible development of elongated centerline grains at low travel speeds must be noted. In welds where this was observed, the transition temperature corresponding to the centerline could not be defined but was probably well above 100°C (212°F). With the present Charpy samples, crack growth was parallel to the welding direction. Initiation of cleavage fracture will depend upon the peak internal stress concentration and hence on the maximum length of dislocation pile-up attainable within the structure (Ref. 12). If this is simply taken to be of the order of the maximum grain dimension perpendicular to the externally applied stress (*i.e.*, roughly 2 mm), then the data in Fig. 15 would imply a DBTT for the weld centerline of about 150°C (302°F).

Determination of the impact toughness of EB welds in ordinary steels is problematic, since the transformation and hardening in the weld area promotes crack deviation away from the plane of the notch (Ref. 13), so that the energy recorded frequently reflects propagation through the relatively low yield strength base metal. Certainly, some instances were observed of crack propagation away from the weld area in the present test program. Nevertheless, from Table 8, weld area hardnesses were not greatly above base metal levels, at least for the higher FF steels, and crack growth in most samples took place generally directly from the notch root, as desired. This is consistent with cleavage resistance and hence weld area toughness in the present steel type being dominated by the local peak ferrite grain size.

It will be noted that toughness does not increase directly with martensite

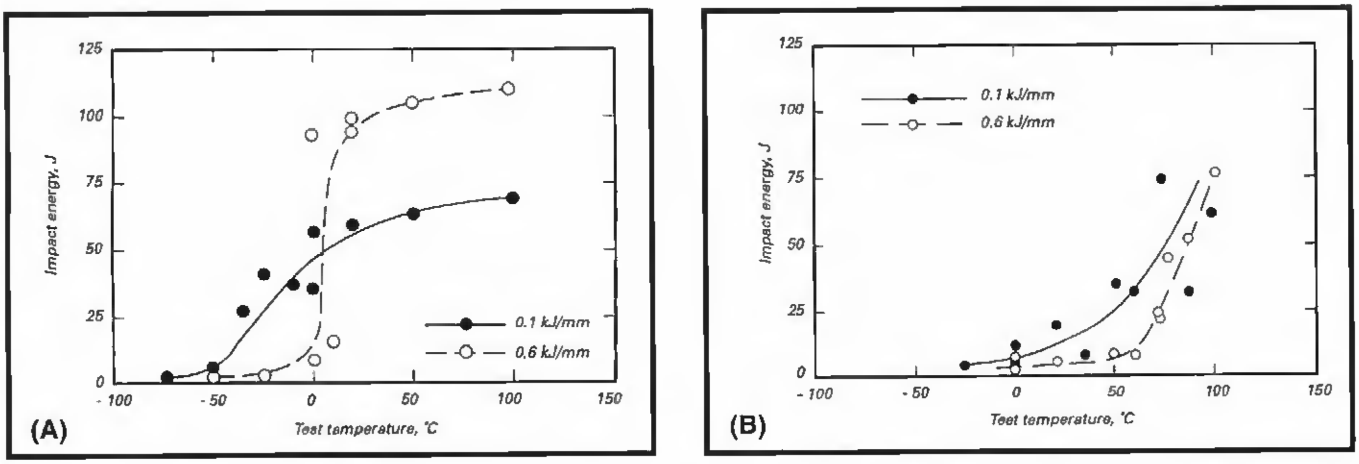

Fig. 11 — Charpy impact results for EB welds at 0.1 and 0.6 kJ/mm. A — 1C849 (FF 7.8); B — 1C850 (FF 10.8).

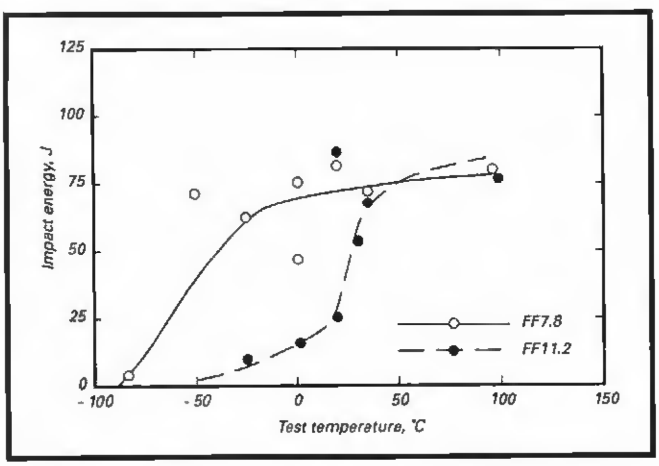

Fig. 12 — Charpy impact results of LFWs in 1C849 (FF 7.8) and 1C857 (FF 11.2).

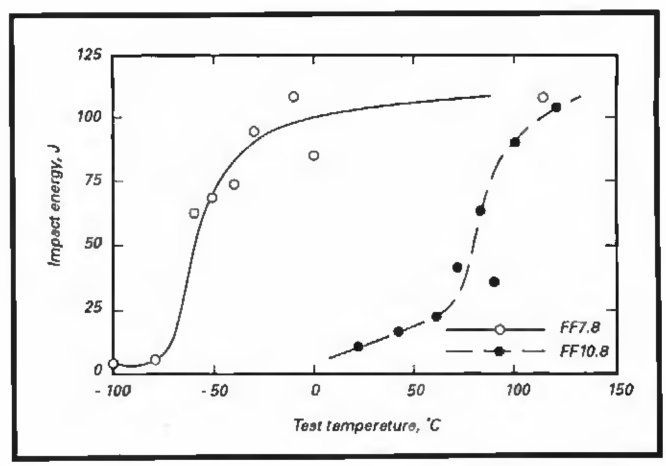

Fig. 13 — Charpy impact results for SMA welds in 1C849 (FF 7.8) and 1C495 (FF 10.8) (Note: 1C495 samples were full size).

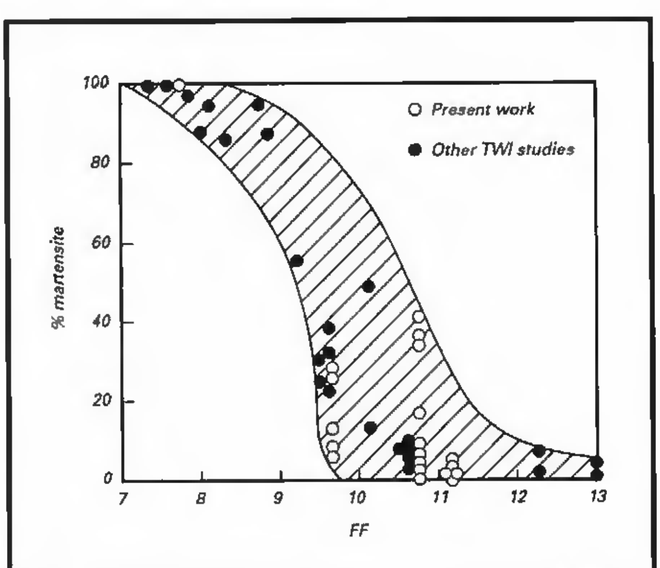

Fig. 14 — Relationship between base steel FF and HAZ martensite content.

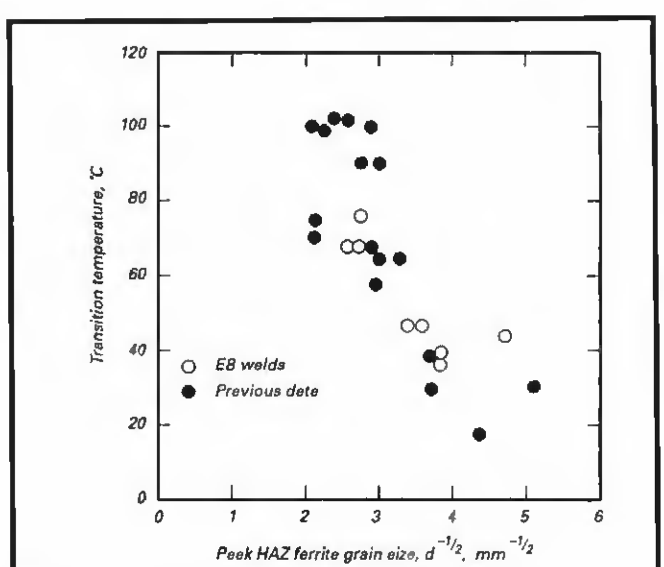

Fig. 15 — Effect of peak ferrite grain size on DBTT.

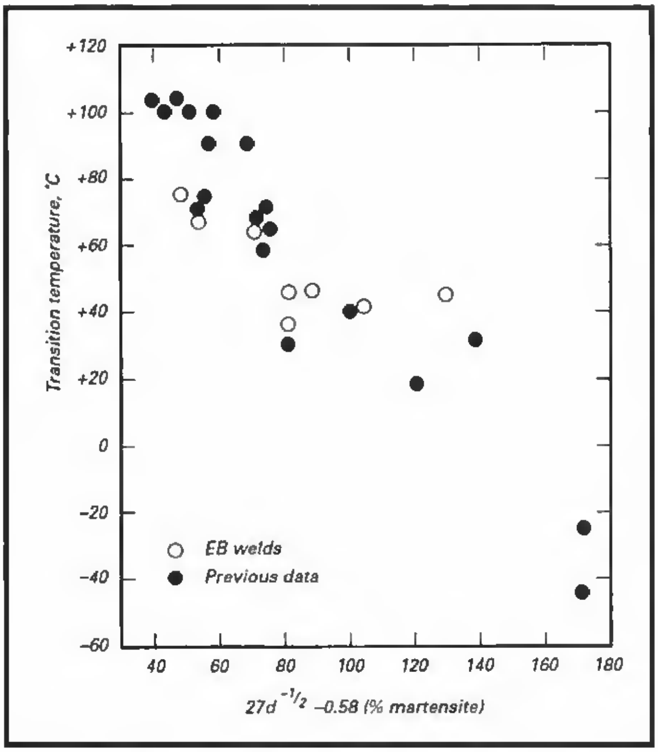

Fig. 16 — Effect of peak ferrite grain size and martensite content on DBTT for steels in which martensite is the minor phase.

level. When ferrite is the major phase, martensite formation may serve to increase the DBTT, presumably by an internal stress concentration effect (Ref. 4), and again the present test results display a similar microstructural dependence to that found for arc weld HAZs — Fig. 16. Nonetheless, there can be no doubt that highest toughness is achieved with a fully martensitic weld region — Fig. 10.

Practical Implications

The present work has confirmed previous findings (Refs. 3–6) that, although low carbon 12%Cr steels may be processed to produce a ferrite/martensite structure in base metal, alloys with a high ferrite factor show a coarse ferrite grain structure on fusion welding. In consequence, a ductile-brittle transition well above normal ambient must be expected, and this must be recognized in practical application of the alloys. The study further confirms that the feasibility of avoiding the problem in high ferrite factor steels by reduction in heat input to the weld is unlikely. In contrast, the fully martensitic structure developed at welds in low ferrite factor materials shows much better toughness. It would still seem that reduction in heat input is preferred, but provided that the associated hardening is acceptable (and, perhaps, that hydrogen cracking is avoided), low ferrite factor steels should offer more general applicability.

From the process viewpoint, the work has illustrated the potential advantage of a forge stage during welding. Reasonable toughness was found for linear friction welds even in fairly high FF steel. It is also clear that beam welding conditions should be carefully controlled to avoid the development of stable centerline grain growth parallel to the welding direction. The effect has been reported in a range of steels (Ref. 9), and can lead to reduced cleavage toughness. In large part, an elongated centerline structure is most likely at travel speeds below the range commonly used in beam welding to maximize joint completion rate, but caution is necessary if lower speeds are employed, for example to avoid solidification cracking.

Summary and Conclusions

Low carbon 12%Cr ferritic/martensitic steels HAZ covering a range of composition and ferrite factor (FF from 7.8 to 11.2) were welded by electron beam and linear friction welding processes. Metallographic examination, hardness and impact testing were carried out, and the following conclusions were reached:

1) With electron beam welding, highest weld area toughness was achieved with low ferrite factor steel (FF = 7.8) giving a fully martensitic weld area; the DBTT was 0°C or below.

2) High ferrite factor steels gave a predominantly ferritic weld area microstructure and resultant DBTT above room temperature.

3) Peak ferrite grain size increased with EB process power for high FF materials; the DBTT depended primarily on the ferrite grain size.

4) Electron beam welding at speeds below about 500 mm/min resulted in elongated centerline grains that showed ready cleavage and DBTT above 100°C (212°F).

5) With linear friction welding, the forge cycle produced a fine transformed structure in the weld area. Even high FF steels gave DBTTs of around 0°C, while a DBTT of about –50°C (–58°F) was observed for low FF fully martensitic material.

Acknowledgments

The authors thank colleagues at TWI for their discussion and assistance in conducting the above program. The work was jointly funded by the Information and Manufacturing Technology Division of the Department of Trade and Industry and the Industrial Members of TWI.

References

1. Hewitt, J. 1992. High-chromium controlled-hardenability steels. INFACON 6. *Proc. 1st International Chromium Steels and Alloys Congress,* Cape Town, Johannesburg, SAIMM, Vol. 2, pp. 71–88.

2. Kreischer, C. G., *et al.* 1961. Welding 12% chromium martensitic stainless steel. *Welding Journal* 40(11): 489-s to 496-s.

3. Castro, R., and de Cadenet, J. J. 1974. *Welding metallurgy of stainless and heat resisting steels.* Cambridge University Press, Cambridge, U.K.

4. Gooch, T. G., and Ginn, B. J. 1990. Heat-affected zone toughness of SMA welded 12%Cr martensitic-ferritic steels. *Welding Journal* 59(12): 431-s to 440-s.

5. Orava , U. H., Karjalainen, L. P., and Kyroelaeinen, A. J. 1993. Impact toughness of heat-affected zone in non-stabilised 12%Cr ferritic stainless steel welds. *Proc. Innovation Stainless Steel,* Associazione Italiana di Metallurgia, Florence, Italy, Vol.2, 2.149–2.154.

6. Jana, S. Effect of varying heat inputs on the HAZ properties of two duplex stainless steels. Vide Ref. 5, Vol. 3, 3.343–3.348.

7. Kaltenhauser, R. H. 1971. Improving the engineering properties of ferritic stainless steel. *Metals Engineering Quarterly,* 41–47.

8. Folkhard, E. 1988. Welding metallurgy of stainless steels. p. 11, Springer-Verlag/Wien, Austria.

9. Komizo, Y., Punshon, C. S., Gooch, T. G., and Blakeley, P. 1986. Effects of process parameters on centreline solidification structure in EB (electron beam) welds. *Met.Con* 18(2): 104R–111R.

10. David, S. A., and Vitek, J. M. 1989. Correlation between solidification parameters and weld microstructures. *International Materials Reviews* 34(5): 213–245.

11. Hsu, S. C., Chakravorty, S., and Mehrabian, R. 1978. Rapid melting and solidification of a surface layer. *Metallurgical Transaction B* 9B 2: 221–229.

12. Smith, E. 1966. The nucleation and growth of cleavage microcracks in mild steel. *Proc. Conf. "Physical basis of field and fracture,"* Inst. of Phys. and Phys. Society, Oxford, pp. 36–46.

13. Elliott, S. 1984. Electron beam welding of C-Mn steels — toughness and fatigue properties. *Welding Journal* 63(1): 8-s to 16-s.